The *rs*-method for material failure simulations

R. Fan and J. Fish

Rensselaer Polytechnic Institute

Troy, NY 12180

Abstract

A new method for propagating arbitrary failure modes is presented. Arbitrary failure modes are resolved on a refined local patch of elements and then embedded into the coarse grid using partition of unity method. Strong discontinuities are propagated by means of element erosion in the superimposed patch of elements only. The method, coined as the *rs*-version of the finite element method (or reduced order *s*-method), has been integrated in ABAQUS and verified on several test problems.

Keywords: multiscale, crack propagation, element erosion, partition of unity

1. Introduction

Studies of causes and mitigation of material failure have been and still are one of the most important subjects in scientific and engineering community. The number of papers, workshops and conferences focusing on this subject are still on the rise; a recent Google search of the key-word "material failure" provided over 59 million hits. Indeed, material failure comes in different shapes and forms: defect nucleation and growth, coalescence, micro-cracking, macro-crack growth, shear banding, just to mention a few. The challenges are in both understanding the mechanisms of material failure and its computational modeling. In this article, we focus on the latter.

From computational point of view, the main difficulty stems from the multiscale nature of failure. Even if failure mechanisms of bond breaking at a discrete scale, defect nucleation and growth, shear banding and macro-fracture leading to catastrophic structural failure were well understood, the so-called formidable "tyranny of scales" coined by the NSF Simulation Based Engineering Science (SBES) report [1], poses tremendous challenges. Limiting the discussion to continuum scales only, our plan is to first briefly review existing practices and then outline our vision for new opportunities culminating in the proposed method.

Finite element modeling of fracture propagation has traditionally been performed by remeshing and by inserting crack surfaces along a crack path allowing the adjacent elements to separate [2]. While complete remeshing of large models may overshadow the entire computational cost, mesh modification, which is local remeshing [3], provides an attractive alternative. In case of dynamic fracture, external time-varying tractions are often applied along crack surfaces to reduce the effect of waves generated by creation of new surfaces [4].

The extended finite element method (X-FEM) pioneered by Belytschko and his associates [5][6] alleviates the need for remeshing of crack surfaces. X-FEM allows the crack to pass arbitrarily through elements by incorporating enrichment functions through the notion of local partition of unity. X-FEM is in particular attractive when used in conjunction with the level set method pioneered by Osher and Sethian [7]. The level set representation of the crack simplifies the selection of the enriched nodes, as well as the definition of the enrichment functions.

Strouboulis et al. [8] have used the partition of unity framework (PUM [9]) to model holes and cracks in two-dimensions, whereas Duarte et al. [10] have studied the simulation of three-dimensional dynamic crack propagation. Alternatively, local enrichment schemes where various failure mechanisms including discontinuity in strains [11,12,13], curvatures [14] and displacements [15,16] can be embedded at the element level. Cohesive elements that allow for separation along element boundaries [17,18] provide an attractive alternative since they do not require enrichment. The nonsmooth crack growth in this case can be attributed to nonsmooth fracture surfaces provided that the mesh is sufficiently fine.

Another category of methods that alleviates the need for remeshing is often known as mesh-free formulation. Methods belonging to this category include: Smooth Particle Hydrodynamics (SPH) originally developed by Gingold [19] and Lucy [20], Element Free Galerkin Method (EFGM) [21], Reproducing Kernel Particle Method (RKPM) [22] and various variants of these methods.

Despite significant progress in understanding and developing various methods for propagating strong and weak discontinuities, commercialization of these technologies has been rather slow. Notable exceptions are fracture codes based on local mesh modification (FRANC3D [23,24]) and Smooth Particle Hydrodynamics (EPIC [25]). Most of the commercial explicit Lagrangian codes, such as LS-DYNA and ABAQUS employ the erosion element algorithm, where element deletion is controlled by certain local failure criterion. The attractiveness of this technology stems from its simplicity. In fact, this technology results in CPU time decrease since fracture often appears in highly deformed elements. The method is accurate provided that sufficiently small elements and adequate erosion criterion are used. One of its drawbacks stems from the mass loss - the effect of which is very severe for large elements, but could be partially circumvented by associating masses with nodes. The element erosion based on local critical stress or strain criterion is known to suffer from mesh size dependency, but energy based failure criterion [26], have shown to yield mesh size independent results [27]. The energy based failure criterion necessitates calculation of path dependent integrals (in dynamics), which have limited the implementation to two-dimensional settings.

We now outline our vision for the next-generation failure simulation code. First, we believe it should have a hierarchical multilevel structure so that failure modes associated with various scales can be hierarchically introduced. By hierarchy, we mean that fine scale features could be introduced without modifying the coarse scale model. Hierarchical structure allows reuse of coarse model meshes and computations and is consistent with a multigrid philosophy. Secondly, failure characteristic are often very complex consisting of interacting weak and strong discontinuities. Therefore, failure modes should not be *a priori* defined, but rather computationally resolved possibly in a auxiliary local patch and then hierarchically introduced into coarse scale. Finally, the technology should be simple, preferably compatible with commercial software architectures.

We now describe one such candidate that possesses aforementioned characteristics. As a multilevel scheme we choose the multilevel s-version of the finite element method [28], which was originally introduced for two levels in [29, 30]. The *s*-method consists of overlaying a basic coarse mesh with a hierarchy of local patches [31] engineered of resolving local features. For instance, the base coarse mesh can be crack free, whereas the discontinuity can be embedded in the superimposed mesh(es) only [32]. Interesting variants of this approach have been recently reported in [33] and [34]. The s-version, however, suffers from two shortcomings: (i) the computational complexity and (ii) the need for remeshing the superimposed mesh. While sufficiently fine superimposed meshes are capable of resolving any failure characteristics, they may involve many more degrees-of-freedom than, for instance, XFEM. The computational complexity of the superimposed mesh can be reduced in several ways. One possibility is to carry out modal analysis in the superimposed patch(es) and then to enrich the coarse scale approximation by critical modes capturing failure characteristics. This obviously has to be repeated with failure evolution. If failure modes extend over many coarse scale elements, it might be advantageous to project these modes onto local supports of the coarse mesh (PUM), to preserve sparsity at the expense of additional degrees of freedom. To remedy the need for remeshing the superimposed patches and to take advantage of commercial software architectures we will employ element erosion technology with a simplified energy based element erosion criterion in the superimposed patches only. The resulting method will be termed as the *rs*-version of the finite element method, or reduced order s-version with element erosion.

The outline of this paper is as follows: The basic idea of the *rs*-method is outlined in Section 2. Section 3 details the formulation, algorithmic details and implementation in ABAQUS. A simplified variant of the energy release-based failure criterion is given in Section 4. Numerical examples are given in Section 5. Conclusion and future research directions conclude the manuscript.

2. The Basic Idea

As a prelude, we start with a brief overview of a two-level structured *s*-version. In the structured *s*-version, which has found its commercial implementation in COMET-AR

[35], element boundaries of the base (underlying) mesh coincide with those of the superimposed elements as shown in Figure 1. This provides considerable simplification in integration of finite element matrices at the expense of optimal placement of the superimposed patch typically placed in the critical regions identified by some error indicators [29].

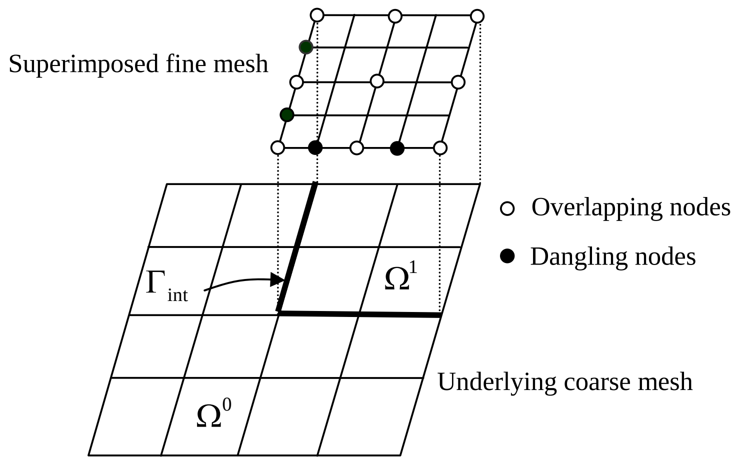

Figure 1: A two-level mesh superposition

The displacements in the superimposed region are approximated as:

$$u_i(x) = \begin{cases} u_i^0(x) = N_I^0(x) d_{Ii}^0 \quad \text{on} \quad \Omega^0 \\ u_i^0(x) + u_i^1(x) = N_I^0(x) d_{Ii}^0 + N_J^1(x) d_{Ji}^1 \quad \text{on} \quad \Omega^1 \end{cases} \tag{1}$$
$$u_i^1(x) = 0 \quad \text{on} \quad \Gamma_{\text{int}}$$

where the superscripts denote the mesh level; lower case subscripts denote spatial dimensions and capital subscripts denote node numbers; summation convention is employed over repeated subscripts (both spatial dimensions and nodes). In Eq. (1), $\Omega^0 \equiv \Omega$ is the entire problem domain and Ω^1 the domain of the superimposed patch. At the interface Γ_{int} between the two meshes the displacement in the superimposed mesh $u_i^1(x)$ are imposed to vanish to ensure C^0 continuity of the solution. Consequently, at the discrete level, the nodes on Γ_{int}, termed as dangling nodes, are constrained, i.e. $d_{Ji}^1 = 0$; n^0 and n^1 represent the number of mesh nodes in the two meshes, respectively. Displacements in the underlying and superimposed meshes are discretized in terms of shape functions denoted as N_I^0 and N_I^1, respectively. Linear dependency is eliminated by constraining the so-called "overlapping" nodes in the superimposed mesh, i.e. the superimposed mesh nodes, which coincide with the underlying coarse mesh nodes as shown in Figure 1.

For the *rs*-method, the displacements in the superimposed region are approximated as:

$$u_i(x) = \begin{cases} N_I^0(x) d_{Ii}^0 \quad \text{on} \quad \Omega^0 \\ \underbrace{N_I^0(x) d_{Ii}^0}_{u_i^0} + \underbrace{N_J^0(x) \Phi_{Ni}^1(x) d_{JN}^1}_{u_i^1} \quad \text{on} \quad \Omega^1 \end{cases}$$
$$d_{JN}^1 = 0 \quad \text{on} \quad \Gamma_{int} \tag{2}$$

where $\Phi_{Ni}^1(x)$ is N^{th}-mode displacement component in the spatial direction i. The modes $\Phi_{Ni}^1(x)$ are selected to be the lowest eigenmodes (excluding rigid body) computed in the superimposed mesh. An alternative weak compatibility condition, detailed in Section 4, has been found to provide superior accuracy.

To illustrate the basic idea of the reduced order method (*rs*-method) we consider a one-dimensional model problem as shown in Figure 2 where discontinuity is modeled by double nodes in the superimposed mesh. For comparison with the *s*-method, we use the same underlying and superimposed meshes. The shape functions and the displacement fields are shown in Figure 3. We select a single non rigid-body mode, which obviously captures the discontinuity as shown in Fig. 4a. It can be seen that for this model problem this mode is identical to the discontinuous piecewise constant function *a priori* constructed in XFEM. The resulting enrichment functions, $N_I^0(x)\Phi_1^1(x)$, are shown in Figure 4b.

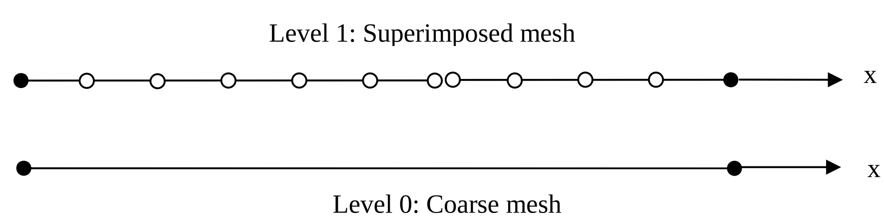

Figure 2: The model problem

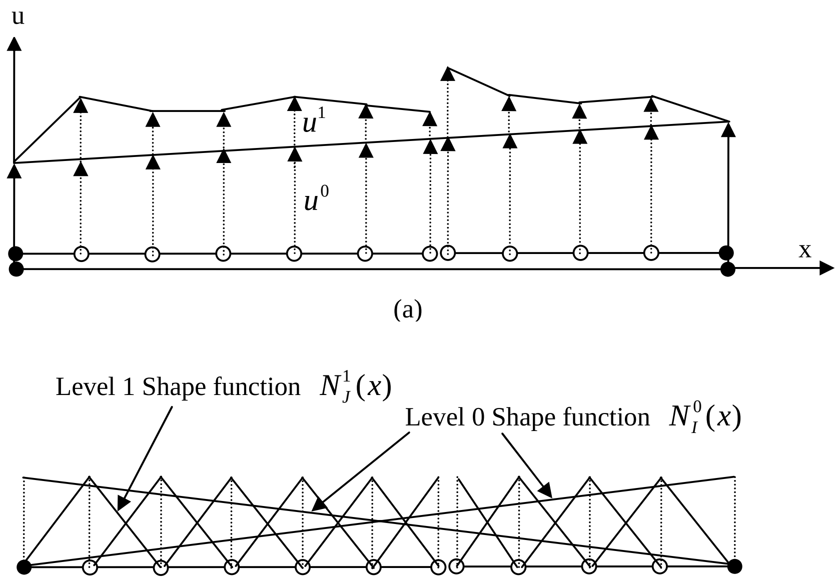

Figure 3: (a) displacement field in the 0 and 1 level meshes, (b) corresponding shape functions in the two meshes

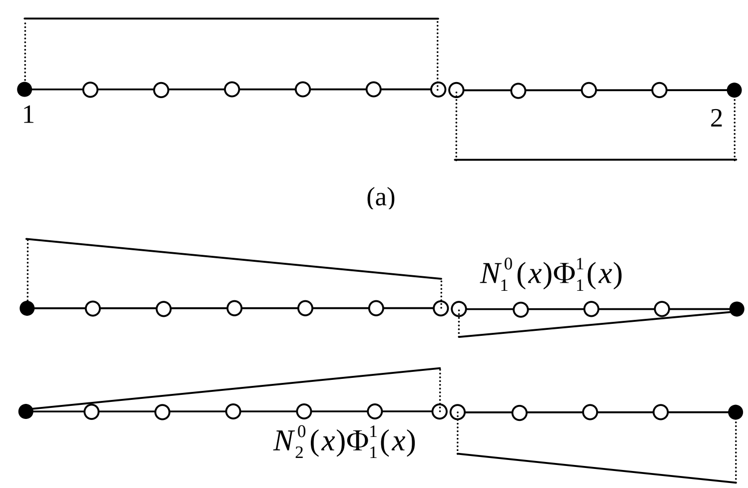

Figure 4: (a) Lowest frequency eigenmode Φ_1^1, (b) corresponding enrichment functions

$N_I^0(x)\Phi_1^1(x)$

3. The Formulation

Consider a problem domain Ω with boundary Γ, consisting of the prescribed displacement boundary Γ_u and the prescribed traction boundary Γ_t. The strong form is given by

$$\begin{aligned}
&\frac{\partial \sigma_{ji}}{\partial x_j} + b_i = 0 \quad \text{on} \quad \Omega \\
&n_j \sigma_{ji} = \bar{t}_i \quad on \quad \Gamma_t \\
&u_i = \bar{u}_i \quad on \quad \Gamma_u
\end{aligned} \tag{3}$$

In local regions where failure takes place at a certain time instant *t*, patch(es) $\Omega^1(t)$ designated to resolve failure characteristics (weak and strong discontinuities) are superimposed as shown in Figure 5. For simplicity, we focus on a two-level scheme.

The weak form is obtained in a usual manner. It seeks for $u_i \in U$ such that

$$\int_\Omega w_{i,j} \sigma_{ij} \mathrm{d}\Omega = \int_{\Gamma_t} w_i t_i \mathrm{d}\Gamma + \int_\Omega w_i b_i \mathrm{d}\Omega \qquad \forall w_i \in U_0 \tag{4}$$

where

$$\begin{aligned}
&U = \{u_i \mid u_i \in H^1, u_i = \bar{u}_i \text{ on } \Gamma_u\} \\
&U_0 = \{w_i \mid w_i \in H^1, w_i = 0 \text{ on } \Gamma_u\}
\end{aligned} \tag{3}$$

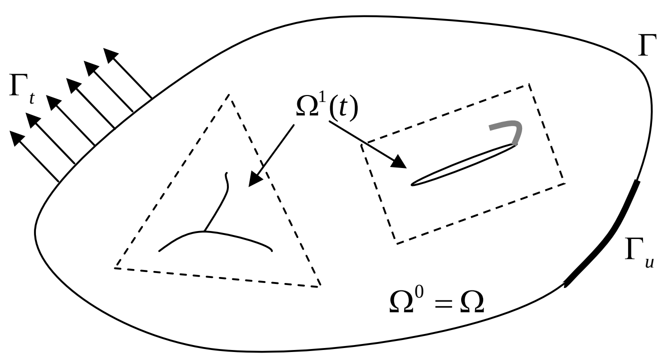

Figure 5: Definition of a local patch $\Omega^1(t)$ at time *t*

The weight functions are decomposed and discretized similarly to the trial functions given in Eq. (2)

$$\begin{aligned}
&w_i(x) = \begin{cases} w_i^0 = N_I^0(x) a_{Ii}^0 \quad \text{on} \quad \Omega^0 \\ w_i^0 + w_i^1 = N_I^0(x) a_{Ii}^0 + N_I^0(x) \Phi_{Ni}^1(x) a_{IN}^1 \quad \text{on} \quad \Omega^1 \end{cases} \\
&w_i^0 = w_i^1 = 0 \quad \text{on} \quad \Gamma_u \\
&w_i^1 = 0 \quad \text{on} \quad \Gamma_{int}
\end{aligned} \tag{5}$$

The resulting discrete equations are summarized below

$$
\begin{aligned}
r_{Ii}^{0} &= \int_{\Omega} \frac{\partial N_I^0}{\partial x_j} \sigma_{ij} \mathrm{d}\Omega - \int_{\Gamma_t} N_I^0 \bar{t}_i \mathrm{d}\Gamma - \int_{\Omega} N_I^0 b_i \mathrm{d}\Omega = 0 \\
r_{Ni}^{1} &= \int_{\Omega^1} \frac{\partial\left(N_I^0 \Phi_{Ni}^1\right)}{\partial x_j} \sigma_{ij} \mathrm{d}\Omega - \int_{\Gamma_t} N_I^0 \Phi_{Nj}^1 \bar{t}_i \mathrm{d}\Gamma - \int_{\Omega^1} N_I^0 \Phi_{Nj}^1 b_i \mathrm{d}\Omega = 0
\end{aligned} \tag{6}
$$

For nonlinear problems, the tangent stiffness matrix is obtained by consistent linearization of (6).

An alternative to the strong compatibility condition (2)b is a weak compatibility given by

$$
\int_{\Gamma_{\text{int}}} \lambda_i u_i^1 d\Gamma = 0 \tag{7}
$$

The function $\lambda_i(x) \in H^0$ is approximated as piecewise constant over element edges Γ_{int}^e (or faces in 3D) positioned at the interface $\Gamma_{\text{int}} = \underset{e}{\cup} \Gamma_{\text{int}}^e$

$$
\lambda_i\ (x) = \sum_{e \in \Gamma_{\text{int}}} N^e \beta_i^e \tag{8}
$$

where

$$
N^e = \begin{cases} 1 & \text{on} \quad \Gamma_{\text{int}}^e \\ 0 & \text{elsewhere} \end{cases} \tag{9}
$$

Substituting (8) and (2) into (7) yields the so-called multi-point constraints (MPC) equations for $d_{IN}^1 \in \Gamma_{\text{int}}$

$$
\sum_{I \in \Gamma_{\text{int}}^e} \sum_{N=1}^{N_{\text{mod}}} N_I^0 \Phi_{Ni}^1 d_{IN}^1 = 0 \quad \forall i, \forall \Gamma_{\text{int}}^e \tag{10}
$$

The MPC condition (10) can be enforced either by using penalty method Lagrange multipliers method or by requiring the weight functions w_i in Eq. (4) to satisfy

$$
\sum_{I \in \Gamma_{\text{int}}^e} \sum_{N=1}^{N_{\text{mod}}} N_I^0 \Phi_{Ni}^1 a_{IN}^1 = 0 \quad \forall i, \forall \Gamma_{\text{int}}^e \tag{11}
$$

To complete the formulation, it remains to address the following two issues: (i) linear dependency between u_i^0 and u_i^1 and (ii) selection of Φ_{Nj}^1. To clarify these issues consider two cases depicted in Figure 6: case A without a crack and case B with a crack. In both cases, the underlying mesh is crack free. The crack is represented in the superimposed mesh (case B) only. For the crack-free case, it is possible that a non-rigid body mode extracted from the superimposed mesh would be linear dependent with a deformation represented by the underlying mesh. In this cases the overlapping nodes I in the superimposed mesh have to be constrained to eliminate linear dependence. On the other hand, if Φ^1_{Nj} captures discontinuity (case B), the underlying crack-free mesh will not represent the same deformation mode. In this case, the overlapping node J is left free. Thus, the strategy for Φ^1_{Nj} extraction is as follows: (i) loop over all the underlying mesh nodes and constrained those, which fall into the category of nodes described in case A (see Fig.6); (ii) extract the lowest energy (excluding rigid body) modes from the superimposed mesh and project them onto local supports, i.e. compute $N^0_I \Phi^1_{Nj}$. In theory, it is possible that $N^0_I \Phi^1_{Nj}$ would show no discontinuity on one or more patches in which the overlapping node has to be constrained.

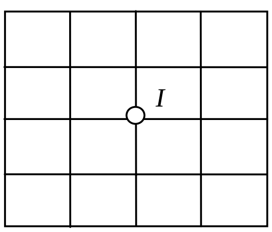

Case A: Superimposed mesh without crack

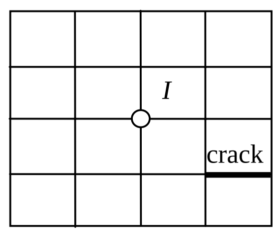

Case B: Superimposed mesh with crack

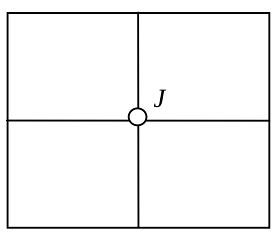

Underlying mesh without crack

Figure 6: Suppressing linear dependency between underlying and superimposed meshes. Node I in the superimposed mesh overlaps node J in the underlying mesh

To this end, we describe the implementation of the *rs*-method in ABAQUS [36]. Our implementation strategy is guided by the limitations of working with commercial software architecture. In ABAQUS, we use a user-defined element subroutine UEL to control the coarse mesh and the superimposed mesh analyses. The basic steps are summarized below:

1. In the first iteration of each load increment, perform modal analysis in the superimposed mesh

$$K^1_{IiJj}\Phi^1_{Jj} = \lambda\Phi^1_{Ii}$$

$$K^1_{IiJj} = \frac{\partial}{\partial d^1_{Jj}}\left(\int_{\Omega^1}\frac{\partial N^1_I}{\partial x_j}\sigma_{ij}\mathrm{d}\Omega - \int_{\Gamma_t} N^1_I\bar{t}_i\mathrm{d}\Gamma - \int_{\Omega^1} N^1_I b_i\mathrm{d}\Omega\right)$$

and store the extracted modes Φ^1_{Ii} in the external file.

2. Read Φ^1_{Ni} from the external file, interpolate for the velocities in the superimposed mesh nodes

$$\dot{u}_i(x^1_I) = \sum_I N^0_I\left(x^1_I\right)\dot{d}^0_{Ii} + N^0_I\left(x^1_I\right)\Phi^1_{Ni}\left(x^1_I\right)\dot{d}^1_{IN}$$

and save them to the external file.

3. Update the stresses in the Gauss points of the superimposed mesh and those in the coarse mesh elements not overlapped by the superimposed mesh.

4. Calculate the residuals based on Eq. (6), compute the tangent stiffness matrix as

$$\begin{bmatrix} \dfrac{\partial r^0_{Ii}}{\partial d^0_{Jj}} & \dfrac{\partial r^0_{Ii}}{\partial d^1_{JM}} \\ \dfrac{\partial r^1_{IN}}{\partial d^0_{Jj}} & \dfrac{\partial r^1_{IN}}{\partial d^1_{JM}} \end{bmatrix}$$

and iterate (Newton or related method) until convergence.

Note that once the enrichment shape functions are defined based on Eq. (2) the last step is carried out automatically by a commercial software of choice.

4. A simple energy-based element erosion criterion

We start from a classical definition of the fracture toughness (or critical energy release rate) G_c as the work required to close a crack by a small increment as shown in Figure 7a.

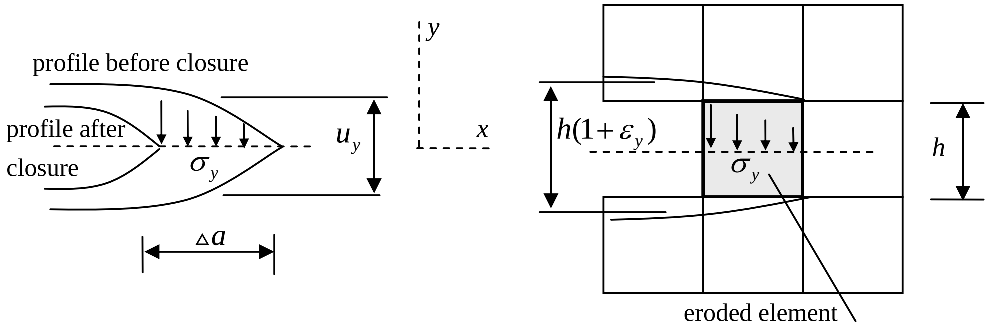

Figure 7: Crack closure tractions and displacements (a) in the analytical model, and (b) in a mesh simulated by element erosion

In the classical fracture mechanics the fracture toughness is defined as

$$G_c = \lim_{\triangle a \to 0} \frac{1}{\triangle a} \int_0^{\triangle a} \frac{1}{2} \sigma_y u_y dx \tag{12}$$

where σ_y is stress normal to the crack surface and u_y is a closure displacements.

We now consider an approximation to the fracture toughness $\tilde{G}_c$ obtained by element erosion. For simplicity, we assume the state of constant element stresses evaluated at the element centroid (one-point integration with stabilization [37]). The eroded element elongation perpendicular to the crack surface is given by $u_y = \varepsilon_y h$ where ε_y is the strain component normal to the crack surface as shown in Figure 7b. If we further assume that the crack propagates normal to the direction of the maximum principal stress in tension σ_1 then Eq. (12) reduces to

$$\tilde{G}_c \approx \frac{1}{2} \sigma_1 \varepsilon_1 h \tag{13}$$

where ε_1 is the normal strain computed in the principal directions of stress. Eq. (13) can be further simplifying for linear isotropic material and by neglecting the remaining principal stress components, which gives

$$\sigma_c = \sqrt{\frac{2\tilde{G}_c E}{h_c}} \tag{14}$$

where h_c is a characteristic material lengthscale (aggregate size, grain size, etc.) and σ_c is a critical stress computed from Eq. (14). The maximum principal stress at which an element of length $h = h_c$ is eroded is then $\sigma_{1er} = \sigma_c$. On the other hand, for elements of size $h \neq h_c$ the critical stress for element erosion is

$$\sigma_{1er} = \sigma_c \sqrt{\frac{h_c}{h}} \tag{15}$$

For instance, if $h_c / h = 2$, i.e., we refine the mesh a by a factor of two, the erosion stress increases by 40% compared to the base mesh ($h = h_c$). The criterion for element erosion (15) is in the spirit of cohesive crack models [38].

<u>Remark:</u> For elements neighboring the crack tip, Eq. (15) has an alternative interpretation. Let r_c be the distance from the crack tip (assumed to be material property) at which the critical stress σ_c is measured. For different meshes, the distance of the element centroid to the crack tip is denoted by r and is of order of element size, i.e, $r \approx h$. Since stresses at the crack tip are varying as $1/\sqrt{r}$, the element erosion stress σ_{1er} is then

$$\sigma_{1er} = \sigma_c \sqrt{\frac{r_c}{r}} \tag{16}$$

Note that Eq. (15) is applicable to all the elements in the mesh, whereas Eq. (16) is limited to elements neighboring the crack tip and would require tracking the crack fronts.

5. Numerical Examples

Our numerical experimentation agenda includes three test problems. First, we investigate the accuracy of the method to predict the stress intensity factor. In the second example, we study quasi-static crack propagation in a concrete beam with energy release-based and stress-based element erosion criteria. Finally, we consider a time dependent impact problem without element erosion.

5.1. Plate with a centered crack

The geometry of the plate with a centered crack is shown in Figures 8a and 8b. The width *w* of the plate is 10cm and the length *L* is 10.25cm. A crack of length 2a=1.0cm is placed at the center. Plane stress condition is assumed with the following material properties: Young's modulus 2.0 GPa and Poisson ratio 0.2. The plate is subjected to mode one tension load of 10.0 MPa. The width of the superimposed patch is 1.25cm and the length is 2.0cm. The global domain is discretized with 40×41 four-node quadrilateral elements; the superimposed patch is placed over 5×8 underlying elements. Each underlying element in the superimposed patch is overlaid by 8×8 four-node quadrilateral elements.

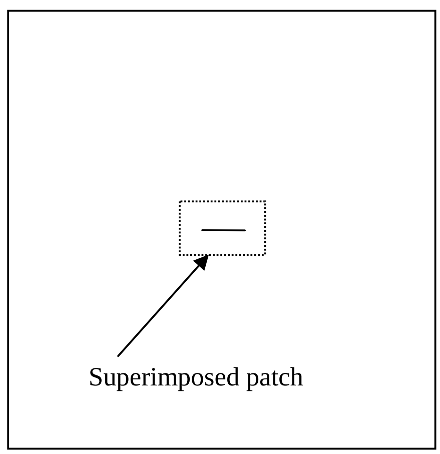

Figure 8a: Plate with center crack

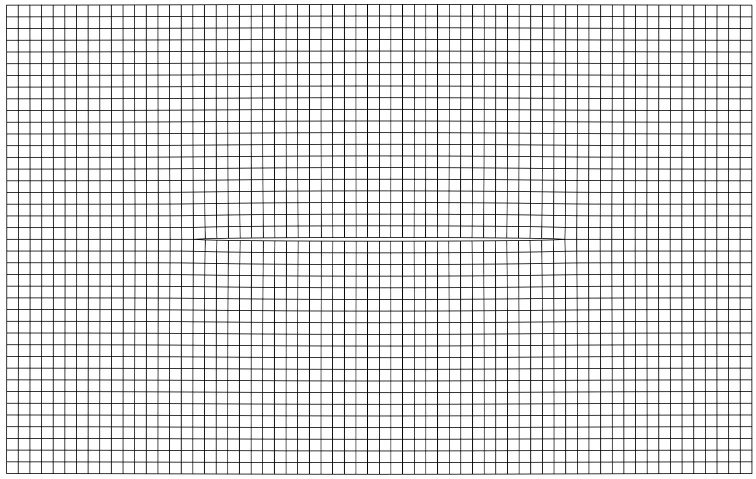

Figure 8b: A superimposed mesh for a plate with a centered crack

Figure 9 gives the error in the stress intensity factor (computed using virtual crack extension method [39]) versus number of modes; both strong and weak compatibility conditions at the interface have been considered. It can be seen that the weak compatibility condition provides superior accuracy at low number of modes, but as the number of modes increases the two methods of enforcing compatibility yield similar performance.

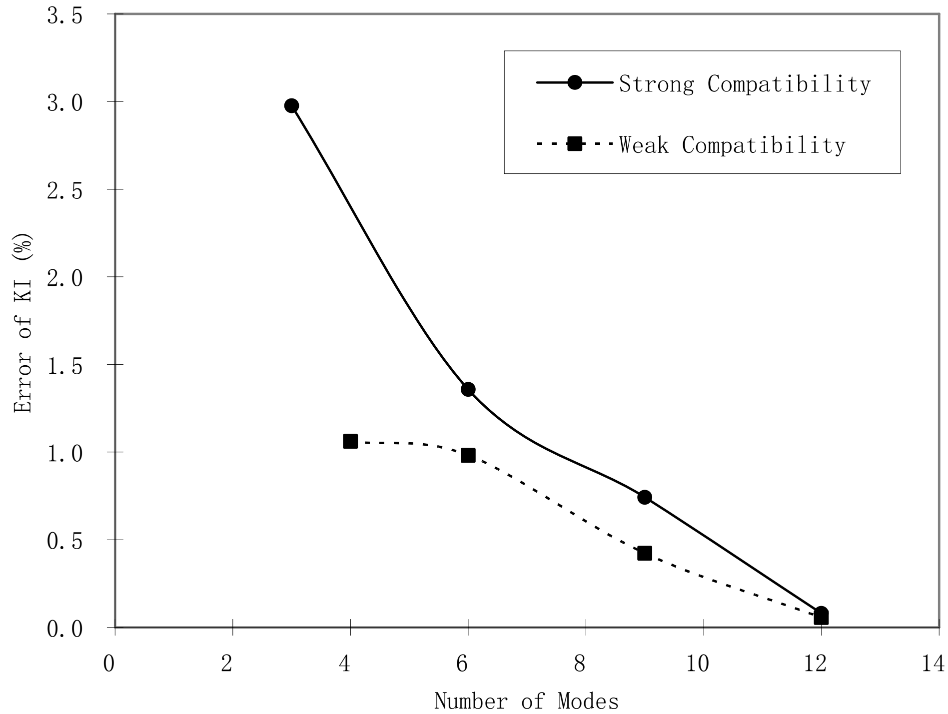

Figure 9: Error in the stress intensity factor versus number of enrichment modes

5.2. <u>Crack propagation in a concrete beam [40]</u>

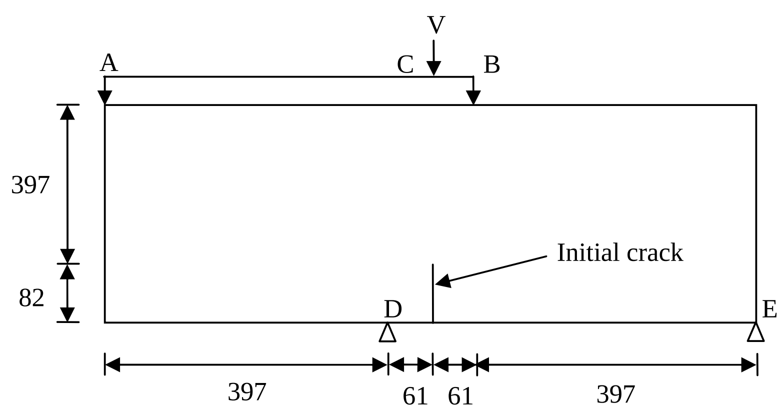

Figure 10: Geometry of notched concrete beam (dimensions in mm)

Consider a beam made of concrete with the following material properties: Young's modulus 24800MPa, Poisson's ration 0.18, and a critical fracture stress 6.0MPa. The geometry and dimensions of the beam are shown in Figure 10. Plane stress is assumed with a beam thickness of 156mm. A linearly increasing velocity is applied at point C starting from 0 to 0.75mm/s with ramping time of 0.38 seconds. The rigid beam AB is used to transmit the load to the concrete beam. We first study the sensitivity of the solution (reaction force at point B versus time and crack height versus time) to the mesh size. Figure 11 depicts the reference mesh, which has 28x24 elements in the refined region at the center. We consider three additional meshes denoted as mesh 1, obtained by splitting each element in the reference mesh into 4 elements, mesh 2 obtained by splitting each element in mesh 1 into 4, and mesh 3 obtained by splitting each element in mesh 2 into 4.

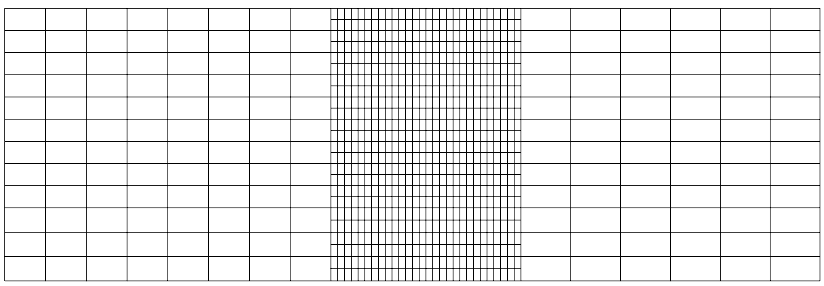

Figure 11: The reference finite element mesh (28x24 elements in the refined region at the center of the beam)

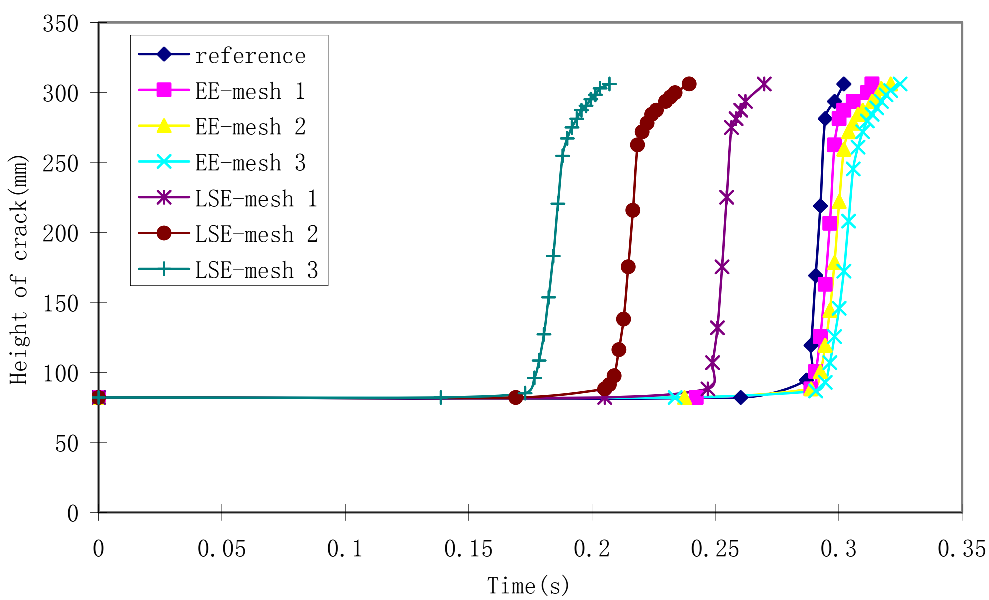

Figure 12: Height of the crack versus time

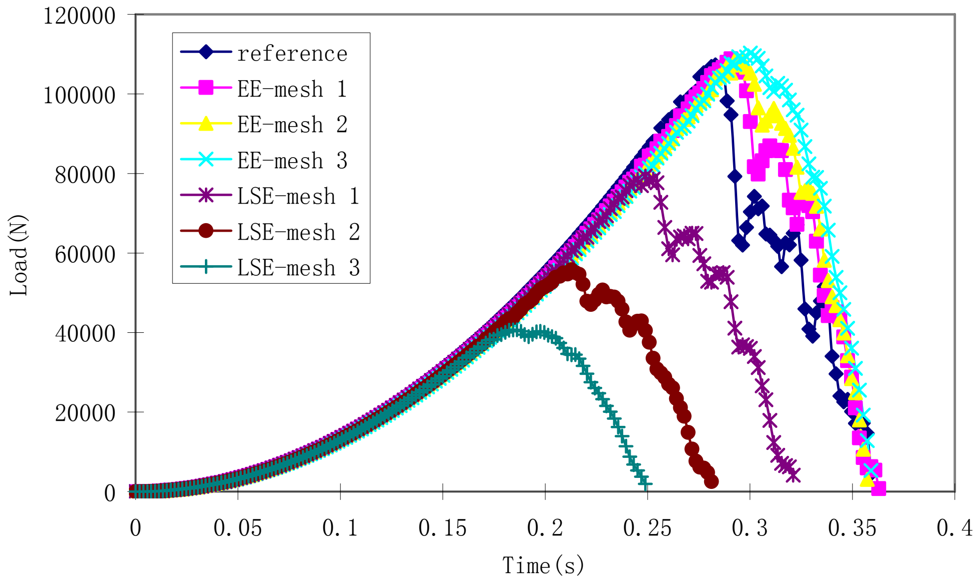

Figure 13: Reaction at support B versus time

We study two failure criteria: (i) local stress-based erosion (LSE) criterion by which an element is removed when the maximum principal stress in tension reaches the fracture stress, and (ii) energy-based erosion (EE) criterion described in Section 4. Figures 12 and 13 depict the height of the crack and the reaction at point B versus time as obtained with the two failure criteria. It can be seen that the local stress-based criterion suffers from significant mesh dependence, whereas energy based criterion is almost insensitive to the mesh size. The finite element meshes of the fully cracked beam as obtained with the energy-based erosion criterion are shown in Figure 14.

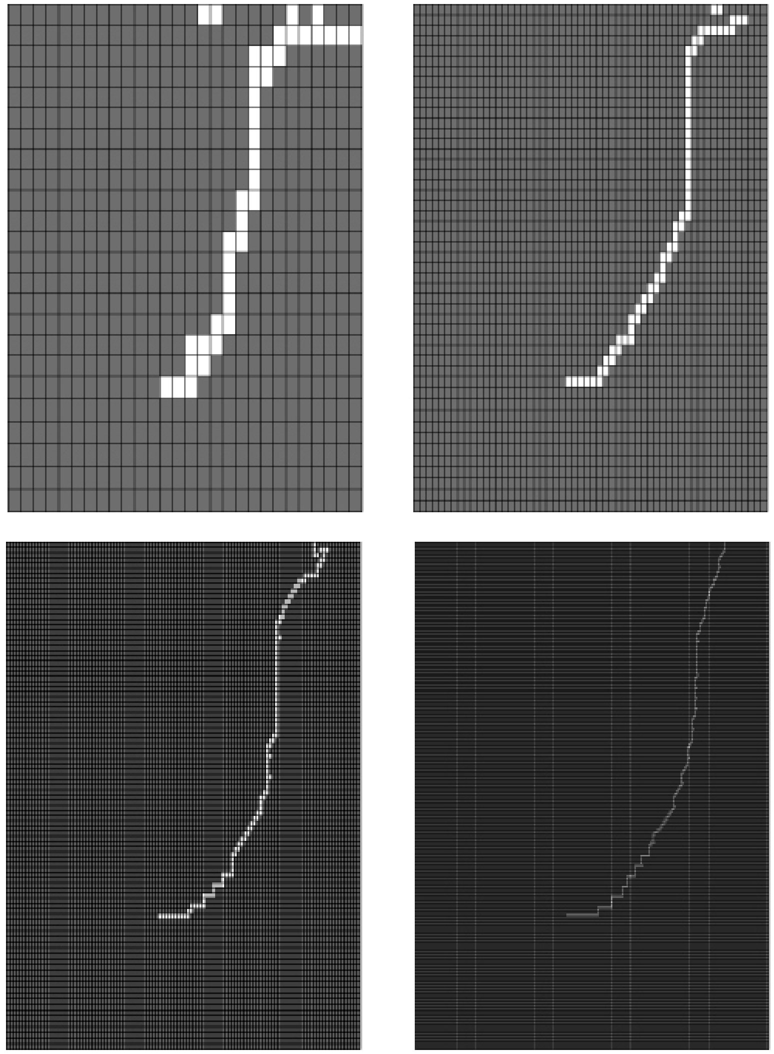

Figure 14: A completely cracked beam as obtained with the energy based erosion criterion in the four meshes

To this end, we study the performance of the *rs*-method for the notched concrete beam. The underlying and the superimposed meshes are shown in Figure 15. 4x4 elements were superimposed on each underlying element crossing the path of the crack as shown in Figure 15b. We considered nine and six modes extracted from the superimposed patch with strong compatibility condition (fewer modes could have been used with weak compatibility). Figures 16 and 17 depict the height of the crack and the reaction at point B versus time as obtained with the rs-method (nine and six modes) and utilizing the energy based failure criteria.

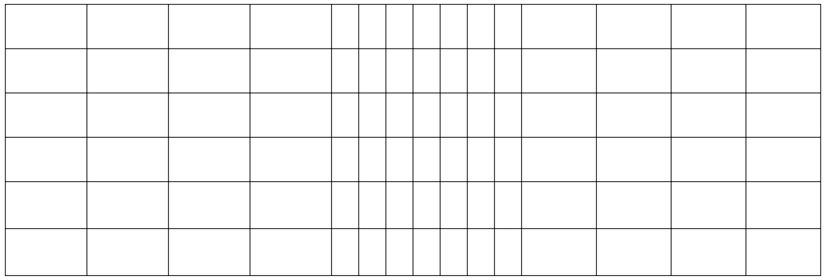

(a)

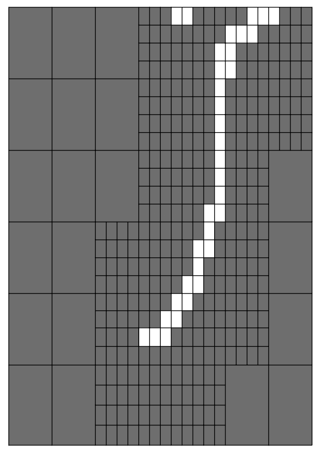

(b)

Figure 15: rs-method: (a) Underlying mesh, (b) snapshots of the propagating crack in the superimposed mesh

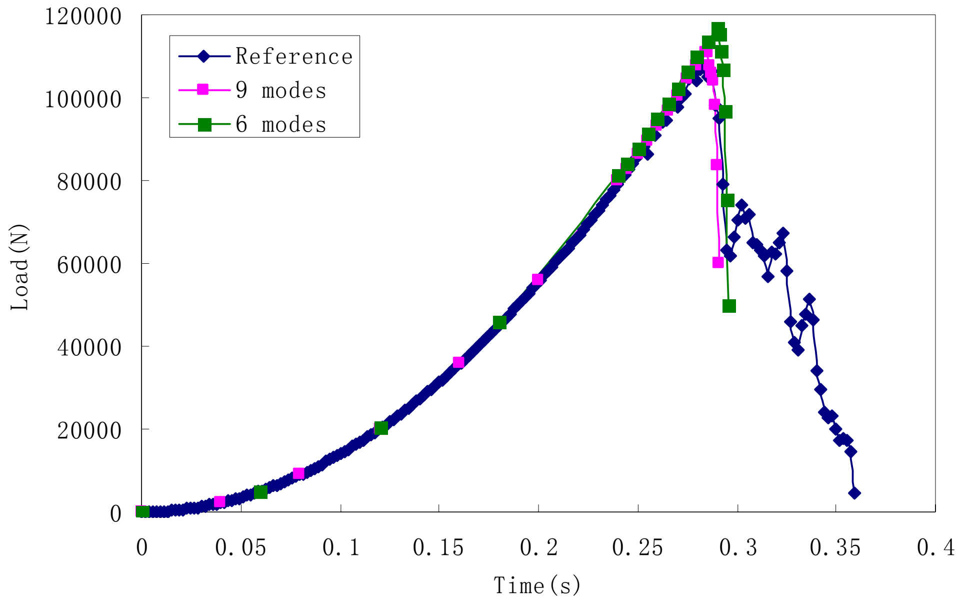

Figure 16: Reaction at support B versus time as obtained with the *rs*-method (six and nine modes) and the reference solution

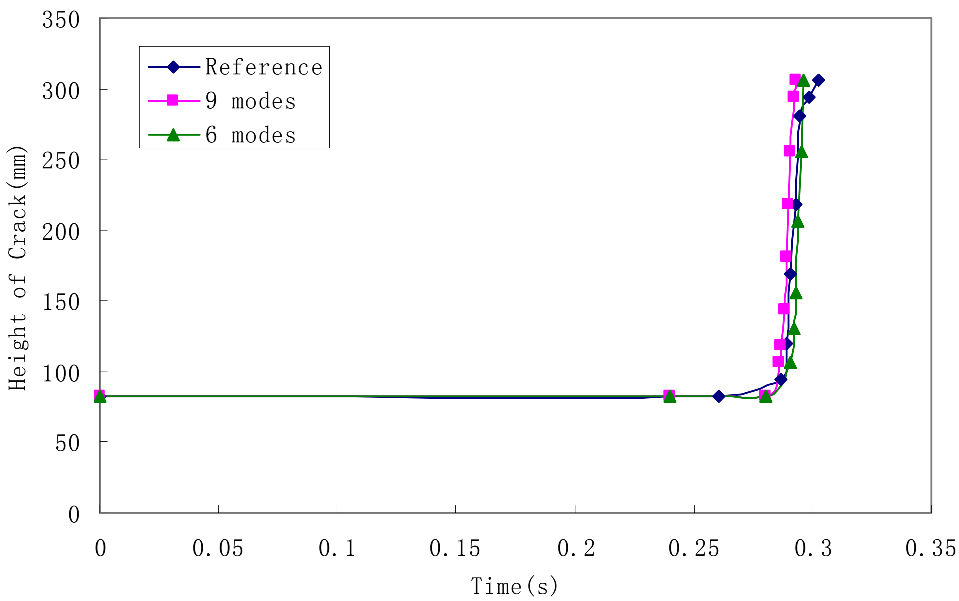

Figure 17: Height of the crack versus time as obtained with the *rs*-method (six and nine modes) and the reference solution

5.3 Impact simulation

In the last example, we study the *rs*-method for impact simulation without element deletion. The length of the beam is 132mm, and the height is 4.83mm. Figure 18 gives the problem setup.

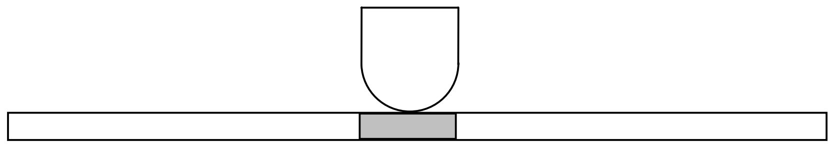

Figure 18: Model problem for impact simulation

The beam is made of DH-36 structural steel with a material model developed by Nemat-Nasser and Guo [41]. The rigid body has a round nose of radius 9mm. The mass of the rigid body is 3% of the mass of the shaded area. The initial velocity of rigid body is 275m/s. Free boundary conditions at the two ends of the beam and plain strain were assumed. Only half of the beam was modeled due to symmetry. The shaded domain under the impactor in Figure 18 shows the placement of the superimposed patch. Three modes were extracted for enrichment.

Figure 19 shows the impactor velocity versus time. An excellent agreement between the reference (no modal reduction) and the *rs*-version is observed.

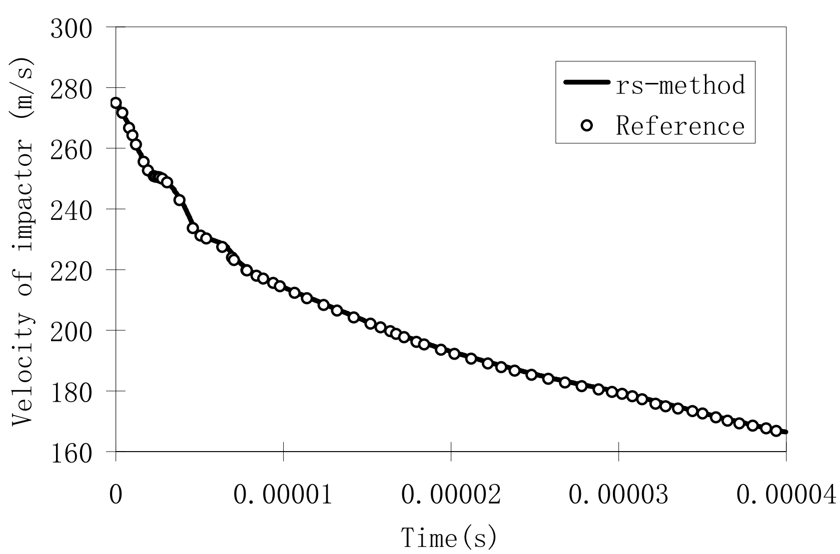

Figure 19: Comparison of the velocity of impactor versus time

5. Conclusions and future research directions

A new method for propagating arbitrary failure modes was developed and verified. The method builds on excellent closely related methods including: XFEM [5], PUM [9], GFEM [8], and *s*-method [30]. We have demonstrated that it is compatible with commecial software architectures by integrating it with ABAQUS.

In the present manuscript, it has been implicitly assumed that a physical dimension of a superimposed patch is much smaller than that of the global problem and that a computational complexity of solving a problem on a single patch is much smaller than solving the global problem. If this were not the case, then it would be instrumental to device an alternative method to eigenmode extraction on a patch. This, for instance, can be accomplished by subjecting a local patch to overall constant and progressively higher order strain fields, similarly to what is done in the homogenization theory, and then to approximate the eigenmodes by a linear combination of solutions obtained on a patch. This issue will be explored in our future work.

Acknowledment: This work was supported by the Office of Naval Research grant number N000140310396 and the Airforce Research Laboaratory grant number 478 -05-506E.

References

1 Simulation - Based Engineering Science, National Science Foundation report sbes0506, http://www.nsf.gov/pubs/reports/sbes_final_report.pdf , May 26, 2006

2 M.S. Shephard, N.B. Yehia, G.S. Burd, and T.J. Weidner. Automatic crack propagation tracking. *Compos. Struct*., Vol. 20, pp.211- 223, 1985.

3 Li, X., Shephard, M.S. and Beall, M.W., 3-D Anisotropic Mesh Adaptation by Mesh Modifications, *Comp. Meth. Appl. Mech. Engng*., Vol. 194(48-49), pp. 4915-4950, 2005

4 R.H. Dodds, M. Tang, T.L Anderson. Numerical procedures to model ductile crack extension. Engng Fract Mech. Vol. 46(2), pp. 253-264, 1993

5 T. Belytschko and T. Black. Elastic crack growth in finite elements with minimal remeshing. *International Journal for Numerical Methods in Engineering* Vol. 45(5), pp. 601– 620, 1999.

6 N. Sukumar, N. Moës, B. Moran, T. Belytschko. Extended finite element method for three-dimensional crack modeling, *International Journal for Numerical Methods in Engineering*, Volume 48, Issue 11 , pp. 1549 – 1570, 2000.

7 S. Osher and J.A. Sethian. Fronts propagating with curvature dependent speed: algorithms based on Hamilton–Jacobi formulations. *Journal of Computational Physics*, Vol. 79(1), pp.12–49, 1988.

8 T. Strouboulis, I. Babuska, K. Copps. The design and analysis of the generalized finite element method. *Comp. Meth. Appl. Mech.Eng*. Vol. 181(1–3), pp.43–69, 2000.

9 J.M. Melenk, I. Babuska. The partition of unity finite element method basic theory and applications. *Comp. Meth. Appl. Mech. Eng*. Vol. 139, pp.289–314, 1996.

10 C.A. Duarte, O.N. Hamzeh, YT.J. Liszka, and W.W. Tworzydlo. The element partition method for the simulation of three-dimensional dynamic crack propagation. *Comp. Meth. Appl. Mech. Eng*., Vol. 119(15–17), pp. 2227–2262, 2001.

11 T. Belytschko, J. Fish and B.E. Engelman, "A finite element with embedded localization zones," *Computer Methods in Applied Mechanics and Engineering*, Vol. 70, (1988), pp. 59 - 89.

12 J. Fish and T. Belytschko, "Elements with embedded localization zones for large deformation problems," *Computers and Structures*, Vol. 30, No. 1/2, (1988), pp. 247-256.

13 M. Ortiz, Y. Leroy, A. Needleman. A Finite-Element Method for Localized Failure Analysis. *Computer Methods in Applied Mechanics and Engineering,* Vol. 61 (2), pp. 189-214, 1987

14 T. Belytschko and J. Fish, "Embedded hinge lines for plate elements," *Computer Methods in Applied Mechanics and Engineering*, Vol. 76, No. 1, (1989), pp. 67-86.

15 F. Armero and K.Garikipati, "An analysis of strong discontinuities in multiplicative finite strain plasticity and their relation with the numerical simulation of strain localization," *International Journal of Solids and Structure*s, Vol. 33, pp. 2863-2885, 1996.

16 J. C. Simo, J. Oliver, and F. Armero, "An analysis of strong discontinuities induced by strain-sofetening in rate-independent inelastic solids," *Computational Mechanics*, Vol. 12, pp. 277-296, 1993.

17 G.T. Camacho and M. Ortiz. Computational modeling of impact damage in brittle materials. *International Journal of Solids and Structures* Vol. 33, pp.2899 –2938, 1996.

18 M. Ortiz and A. Pandolfi. Finite-deformation irreversible cohesive elements for three-dimensional crack-propagation analysis. *International Journal for Numerical Methods in Engineering* Vol. 44, pp. 1267–1282, 1999.

19 R.A. Gingold and J.J. Monaghan. Smoothed particle hydrodynamics: theory and application to non-spherical stars. Monthly Notices Royal Astronomical Society, Vol. 181, pp. 375-389, 1977.

20 L.B. Lucy. A numerical approach to the testing of fusion process. Astronomical Journal, Vol. 88, pp. 1013-1024, 1977.

21 T. Belytschko, Y.Y. Lu, and L. Gu. Element-free Galerkin methods. *International Journal for Numerical Methods in Engineering*, Vol. 37, pp. 229-256, 1994.

22 W. K. Liu, S. Jun, S. Li , J. Adee, T. Belytschko. Reproducing kernel particle methods for structural dynamics. *International Journal for Numerical Methods in Engineering*, Vol. 38, pp. 1655-1679, 1995.

23 B. J. Carter, C.-S. Chen, A. R. Ingraea and P. A. Wawrzynek, 'A topology based system for modeling 3d crack growth in solid and shell structures', in Proc. 9th Int. Congr. on Fracture, Sydney, Australia, Elsevier Science Publishers, Amsterdam, 1997.

24 B.J. Carter, P.A. Wawrzynek, A.R. Ingraffea. Automated 3-d crack growth simulation. *Int. J. Numer .Meth. Eng.* Vol. 47, pp. 229–253, 2000

25 J. R. Johnson, R.A. Stryk, T.J. Holmquist, and S.R. Beissel. Numerical Algorithms in a Lagrangian Code. Report. Wright Laboratory. Elgin Air Force Base, 1997.

26 T. Nakamura, C.F. Shih, L.B. Freund. Computational methods based on an energy integral in dynamic fracture. *Int. J. Fracture*, Vol. 27, pp.229-243, 1985.

27 S.R. Beissel, G.R. Johnsona, C.H. Popelar. An element-failure algorithm for dynamic crack propagation in general directions. *Engineering Fracture Mechanics*, Vol. 61, pp. 407-425, 1998.

28 J. Fish and S. Markolefas, R. Guttal and P. Nayak. On adaptive multilevel superposition of finite element meshes. *Applied Numerical Mathematics,* Vol. 14, pp. 135-164, 1994.

29 J. Fish and S. Markolefas. Adaptive s-method for linear elastostatics. *Comp. Meth. Appl. Mech. Engng.*, Vol. 103, pp. 363-396, 1993.

30 J. Fish. The s-version of the finite element method. *Computers and Structures,* Vol. 43, No. 3, pp. 539-547, 1992.

31 J. Fish and A. Wagiman. Multiscale finite element method for heterogeneous medium. *Computational Mechanics: The International Journal*, Vol. 12, pp.1-17, 1993.

32 J. Fish. Hierarchical modeling of discontinuous fields. *Communications in Applied Numerical Methods*, Vol. 8, pp. 443-453, 1992.

33 S. Lee, J. Song, Y. Yoon, G. Zi, T. Belytschko, Combined extended and superimposed finite element method for cracks, *International Journal for Numerical Methods in Engineering*, Volume 59, Issue 8, pp. 1119-1136, (2004)

34 S. Loehnert and T. Belytschko, A multiscale projection method for macro/microcrack simulations, DOI: 10.1002/nme.2001.

35 G. Stanley, I. Levit, B. Stehlin and B. Hurlbut, CSM Task 15 Report, Lockheed, Palo Alto Research Laboratory, 1991.

36 ABAQUS Analysis User’s Manual, 2006.

37 T. Belytschko and I. Leviathan, "Physical Stabilization of the 4-node Shell Element with One Point Quadrature," *Computer Methods in Applied Mechanics and Engineering*, 113, 321-350 (1994)

38 Hillerborg A, Modeer M, Petersson P E. Analysis of crack formation and crack growth in concrete by means of fracture mechanics and finite elements. *J. Cement and Concrete Research*, 1976,6 (6): 773–782.

39 D.M. Parks. The Virtual Crack Extension Method for Nonlinear Material Behavior. *Computer Methods in Applied Mechanics and Engineering*, Vol. 12, pp. 353–364, 1977.

40 ABAQUS Benchmarks Manual, 2006.

41 S. Nemat-Nasser and W.G. Guo. Thermomechanical response of DH-36 structural steel over a wide range of strain rates and temperatures. *Mechanics of Materials*, Vol 35, pp 1023-1047, 2003.